SECTOR-BASED FINITE-SET MODEL PREDICTIVE CONTROL OF THREE-LEVEL GRID-CONNECTED INVERTERS

Yuanyi LIU[1]

In order to address the issue of imbalance in the midpoint voltage of a three-level grid-connected converter and enhance control performance and output quality, we propose a novel approach utilizing finite set switch state predictive control. Firstly, we establish a mathematical model for the three-level grid-connected inverters and introduce the finite set switch state model to accurately depict its dynamic behavior. Secondly, we employ a simplified model predictive control algorithm, based on sector division, to calculate the optimal switch state sequence and achieve closed-loop control of the output current. Finally, we conduct simulation experiments to validate our proposed method. The results of these experiments demonstrate the effectiveness of our approach in accurately controlling the voltage and current of the three-level grid-connected converter and effectively mitigating the imbalance in the midpoint voltage.

Keywords: Neutral-point-clamped three-level inverter, Model predictive control, Sector-based finite-set model predictive control, Common mode voltage balance, Cost function

1. Introduction

With the rapid development of power electronics technology, the three-level Neutral-Point-Clamped (NPC) inverter, as a high-performance, high power density inverter structure, has been widely applied in renewable energy generation systems, AC motor drives, and other fields. This inverter's individual switching devices bear a smaller voltage stress, making it easier to achieve high power or high voltage level output. It has smaller dv/dt, better output harmonic performance, and the grid-connected filter occupies a smaller volume [1-3].

Over the past three decades, Model Predictive Control (MPC) has become a research hotspot both domestically and internationally. Initially, MPC was employed in the field of process control. However, it wasn't until 1983 that scholars introduced it to the realm of power electronics, making it shine brightly in this domain. In recent years, with the rapid advancement of microprocessors, MPC has swiftly become the effective method and key technologies control method for power converters and drives [4-6].

[1] Lingnan Normal University, School of Electronic and Electrical Engineering, Zhanjiang, 524048, China; e-mail: lyy_lou@163.com

A review of existing literature reveals the extensive application of MPC across various sectors within power electronics. For instance, research [7] presented a model-free predictive current control for synchronous reluctance motor drives, addressing their parameter robustness issues. Another study [8] proposed a predictive current control method for permanent magnet synchronous motors, while research [9] introduced a predictive speed control method for the same type of motors. Further, an in-depth exploration of model predictive direct torque control for AC motors was presented in research [10].

In the domain of grid-connected rectification and inversion control, MPC was integrated into two-level power converters by research [11], setting the stage for subsequent applications in power converters. The pioneering work of research [12] implemented MPC in three-level power converters, incorporating controls for output current, neutral point voltage, and switching frequency. The application of model predictive control has also significantly expanded into multilevel converters, as well as in the fields of Uninterruptible Power Supplies (UPS), active power filters, and DC-DC converters, as evidenced by research [13-15].

There are two kinds of model predictive control used in power electronics: Finite-set model predictive control (FCS-MPC) and Continuous-set model predictive control (CCS-MPC). CCS-MPC is a model predictive control containing a PWM modulator, whose predictive controller produces continuous outputs converted into switching states via the modulator. Modulated MPC can achieve multi-objective optimization control, typically including controls for grid current, neutral point voltage, and common mode voltage. However, since this method incorporates a modulator, it's generally challenging to optimize the switching frequency. FCS-MPC, without a modulator, generates a limited number of switching states. It uses these finite states to resolve the optimization problem, selecting the best switch state through a cost function. The optimal switching state obtained is subsequently employed to drive the converter, benefiting from the absence of a modulator. As a result, FCS-MPC exhibits remarkably faster dynamic response characteristics. Additionally, it's easier to embed various constraints into the predictive control algorithm, making FCS-MPC an essential method for solving multi-objective optimization problems [16-20].

The primary goal of this research is to overcome the limitations associated with traditional PID-based PWM control methods when tackling neutral point challenges in a three-level NPC inverter. These challenges include fluctuations in neutral point voltage and increased current harmonics. To this end, a novel FCS-MPC approach is proposed, specifically designed to suppress neutral point voltage and enhance both control performance and output quality of the inverter system. However, it is worth noting that the conventional FCS-MPC control algorithm necessitates multiple loop solutions (27 times) within each sampling period, resulting in significant online computational burden. In order to address this issue,

this paper introduces an improved FCS-MPC control algorithm with neutral point voltage suppression sector division, which notably mitigates the neutral point voltage while reducing the overall online computation. The key finding of this study is that this algorithm can effectively enhance control performance, optimize output quality, and hold significant practical implications.

2. NPC Three-Level Grid-Connected Converter

2.1 NPC Three-Level Inverter Circuit Topology

The circuit topology structure of the NPC three-level inverter is illustrated in Fig. 1. It consists of several components: the DC-side power supply (Udc), voltage dividing capacitors (C1 and C2), three groups of switching bridge arms comprising four power switches each (VT1 to VT4) and two clamp diodes (D1 and D2), an output filter inductor (L), and the midpoint of the DC voltage dividing capacitor (O). Additionally, the neutral point of the grid (N) is connected with a Y-type load [21-23].

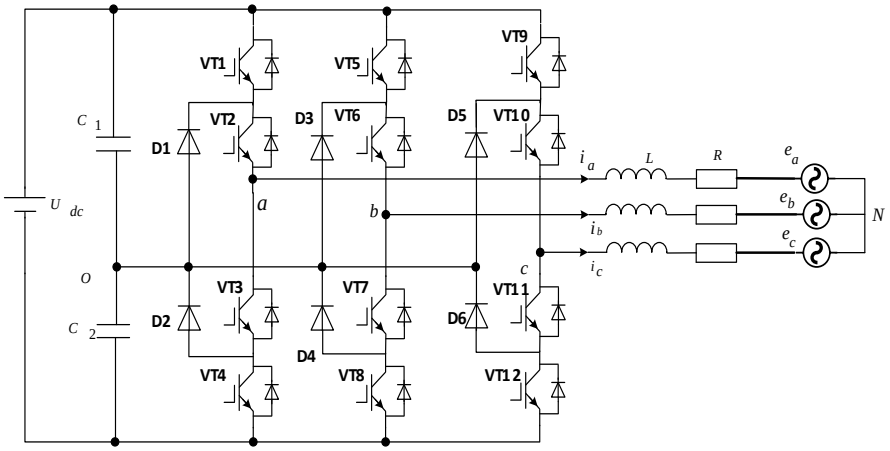

Fig.1. Circuit topology of the NPC three-level inverter.

2.2 State Combinations of NPC Three-Level Inverter

Taking phase A as an example, when the upper bridge arm power switches VT1 and VT2 are on, and the lower bridge arm switches VT3 and VT4 are off, the inverter output is Udc/2, defining the inverter output state as P state at this time. Similarly, as shown in Fig. 2, when the inverter output is 0, it is in the O state, and the output is −Udc/2 in the N state [24-26].

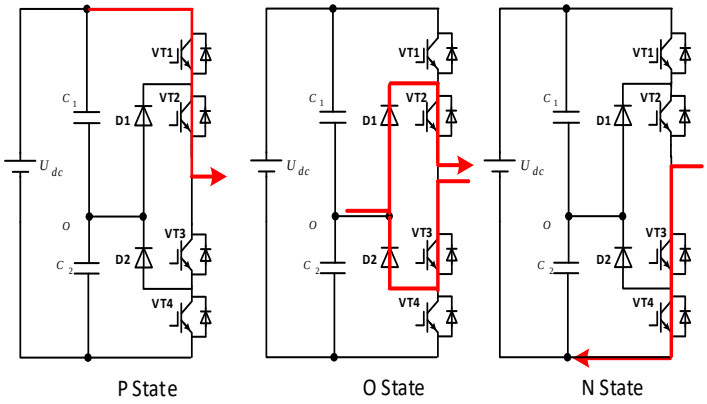

Fig.2. Output state of the NPC three-level inverter.

For analytical purposes, in this context, the switching functions of phases A, phases B, and phases C in the three-level inverter are defined as Sa, Sb, and Sc, respectively. These functions are uniformly denoted by (j=a, b, c), with potential values of -1, 0, or 1, as depicted in Table 1:

Table 1

Relationship between single-phase switch state and output voltage

Output Voltage	*VT1*	*VT2*	*VT3*	*VT4*	*Sa*
Udc/2	1	1	0	0	P(1)
0	0	1	1	0	O(0)
-Udc/2	0	0	1	1	N(-1)

2.3 Space Voltage Vector

The voltage at the inverter's output relative to midpoint O can be represented as:

$$U_{jO} = \frac{U_{dc}}{2} S_j \tag{1}$$

Assuming the system is symmetrical, it can be deduced from (1) that the voltage of the inverter relative to the grid's neutral point is:

$$\begin{bmatrix} U_{aN} \\ U_{bN} \\ U_{cN} \end{bmatrix} = \frac{U_{dc}}{6} \begin{bmatrix} 2 & -1 & -1 \\ -1 & 2 & -1 \\ -1 & -1 & 2 \end{bmatrix} \begin{bmatrix} S_a \\ S_b \\ S_c \end{bmatrix} \tag{2}$$

Thus, the reference voltage vector is defined under equal amplitude conditions as expressed in equation (3):

$$V = \frac{2}{3}(U_{aN} + U_{bN} e^{j\frac{2\pi}{3}} + U_{cN} e^{j\frac{4\pi}{3}}) \tag{3}$$

Transforming the coordinates of equation (3) into the $a\beta$ coordinate system is shown as:

$$V = \frac{U_{dc}}{6}[(2S_a - S_b - S_c) + j\sqrt{3}(S_b - S_c)] \tag{4}$$

Through substituting the 27 switch states of Sa, Sb, and Sc into equation (4), a vector is obtained for each combination, yielding a comprehensive set of expressions for spatial voltage vectors. This set encompasses a total of twenty-seven vectors, consisting of three zero vectors, six large vectors, twelve small vectors, and six medium vectors. These vectors are visualized and represented in the *aβ* coordinate system, as illustrated in Fig. 3:

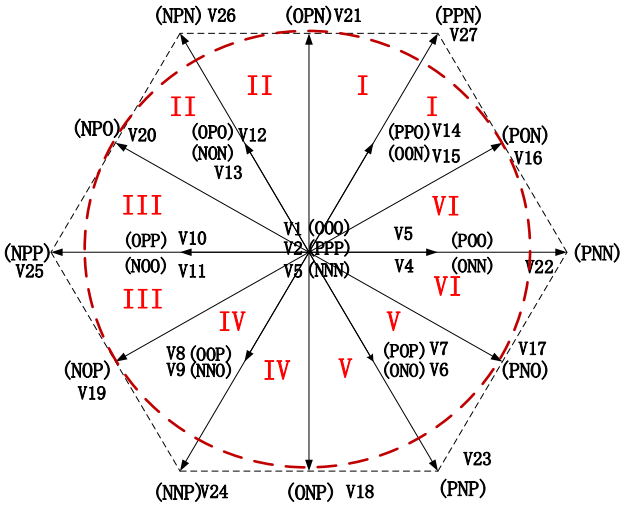

Fig.3. Three-level Vector Diagram

3. Predictive Mathematical Model of the Three-level NPC Inverter

3.1 Predictive Mathematical Model

Combining the topology of the three-level NPC inverter from Fig. 1 with Kirchhoff's law, its mathematical model in the three-phase stationary coordinate system can be represented as (5), where $j = a, b, c$:

$$L\frac{d}{dt}\begin{bmatrix} i_a \\ i_b \\ i_c \end{bmatrix} = \begin{bmatrix} u_{aN} \\ u_{bN} \\ u_{cN} \end{bmatrix} - \begin{bmatrix} u_a \\ u_b \\ u_c \end{bmatrix} - R\begin{bmatrix} i_a \\ i_b \\ i_c \end{bmatrix} \tag{5}$$

Transforming from the stationary abc coordinate system via Clark's transformation to the *α*-*β* two-phase stationary coordinate system, the equation is:

$$L\frac{d}{dt}\begin{bmatrix} i_\alpha \\ i_\beta \end{bmatrix} = \begin{bmatrix} u_\alpha \\ u_\beta \end{bmatrix} - \begin{bmatrix} e_\alpha \\ e_\beta \end{bmatrix} - R\begin{bmatrix} i_\alpha \\ i_\beta \end{bmatrix} \tag{6}$$

The forward Euler discretization is applied to the load current in equation (6):

$$\begin{bmatrix} i_\alpha(k+1) \\ i_\beta(k+1) \end{bmatrix} = \frac{Ts}{L}\begin{bmatrix} u_\alpha(k)-e_\alpha(k) \\ u_\beta(k)-e_\beta(k) \end{bmatrix} + (1-\frac{RT_s}{L})\begin{bmatrix} i_\alpha(k) \\ i_\beta(k) \end{bmatrix} \tag{7}$$

In equation (7), *ia(k+1) and iβ(k+1)* are the predicted output current values at the moment *k+1*, while *ia(k) and iβ(k)* are the output current values at moment *k*.

3.2 Analysis of Midpoint Voltage

NPC three-level inverters are known to experience issues with DC capacitor voltage imbalance. This imbalance in the voltages across the DC side capacitors can result in fluctuations in the midpoint voltage. The imbalance of midpoint voltage is an inherent issue in NPC three-level inverters and may have adverse effects.

The root cause of the imbalance in midpoint voltage is as follows: The NPC three-level inverter comprises twenty-seven vectors, out of which six are large vectors and three are zero vectors, representing the three-phase output connected to the positive and negative DC bus lines, which do not impact the midpoint voltage. However, when employing medium and small vectors, at least one phase output is linked to the zero DC bus line, forming a current loop with the positive (or negative) DC bus line. This loop results in charging and discharging of the DC capacitor, thereby causing fluctuations in the midpoint voltage. [27-29].

As shown in Fig. 4, the midpoint voltage is defined as: *uO=(uc1+uc2)/2*

Where uC1 and uC2 are the voltages across capacitors C1 and C2, respectively.

$$\begin{cases} C\frac{du_{c1}}{dt} = I_{c1} \\ C\frac{du_{c2}}{dt} = I_{c2} \end{cases} \text{ Discretization } \begin{cases} C\frac{u_{c1}(k+1)-u_{c1}(k)}{T_s} = I_{c1} \\ C\frac{u_{c2}(k+1)-u_{c2}(k)}{T_s} = I_{c2} \end{cases} \tag{8}$$

Define the midpoint current *Io*, which satisfies equation (9)

$$I_{c1} - I_{c2} = I_o \tag{9}$$

If the midpoint current is not zero, it is said that the inverter's midpoint voltage is unbalanced:

$$I_o = (1-S_a{}^2)i_a + (1-S_b{}^2)i_b + (1-S_c{}^2)i_c \tag{10}$$

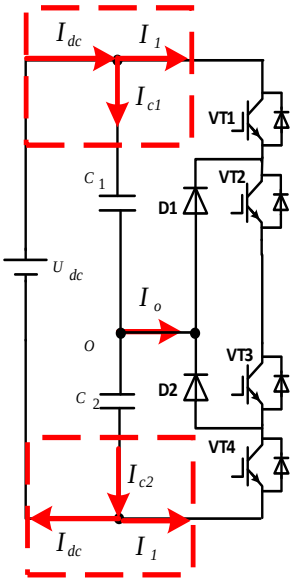

Fig.4. Imbalance Current of Midpoint Voltage

From equations (8) to (10), equation (11) can be derived:

$$\begin{aligned} & u_{c1}(k+1)-u_{c2}(k+1) \\ & = u_o(k)+\frac{T_s}{C}[(1-S_a{}^2)i_a+(1-S_b{}^2)i_b+(1-S_c{}^2)i_c] \\ & = u_o(k+1)=u_o(k)+\frac{T_s}{C}I_o(k) \end{aligned} \tag{11}$$

3.3 Selection of Cost Function

The basic idea of model prediction is to use the predictive model to select an optimal state from all possible states over a few future sampling periods. This state minimizes the cost function. This control algorithm has advantages such as simple theory, changeable constraints, and flexible design options for different control systems.

For the traditional load current FCS-MPC control algorithm, the selected cost function is shown in equation (12)

$$g_j=\left|i_\alpha^*(k+1)-i_\alpha(k+1)\right|+\left|i_\beta^*(k+1)-i_\beta(k+1)\right| \tag{12}$$

Where: *ia*(k+1) and iβ*(k+1)* are the current reference values, *ia(k+1)* and *iβ(k+1)* are the predicted current values. The goal of using the current model predictive control is to stabilize the output current control.

To meet the objectives of both current control and midpoint voltage control, it's necessary to reconstruct the cost function.

$$g_j = \left|i_\alpha^*(k+1) - i_\alpha(k+1)\right| + \left|i_\beta^*(k+1) - i_\beta(k+1)\right| + \lambda\left|0 - u_o(k+1)\right| \tag{13}$$

Where: λ is the weighting coefficient for midpoint voltage balance control. By adjusting the value of λ, midpoint balance control can be achieved.

4. FCS-MPC Control Algorithm

4.1 Traditional FCS-MPC Control Algorithm

The conventional FCS-MPC algorithm is a model predictive control-based optimization algorithm utilized for real-time control of systems. Its essential steps can be summarized as follows [30-31]:

(1) System Modeling: First, a mathematical model, such as a state-space model or transfer function model, is established for the system to be controlled. This model reflects the dynamic behavior and input-output relationship of the system.

(2) Prediction Problem: At the beginning of each control cycle, the known system model and current state information are used to predict the system's behavior over a future period. This usually involves discretizing the system model and calculating predicted states and outputs based on the current state.

(3) Optimization Problem: The prediction problem is transformed into an optimization problem. The goal is to find a set of optimal control inputs to minimize specific performance metrics. These metrics could be related to tracking errors, energy consumption, system stability, and other criteria.

(4) Constraint Conditions: Within the optimization problem, system constraints, such as input limitations, output constraints, or inherent system constraints, must be considered. These constraints help ensure that the chosen control inputs are within a safe range and prevent system overloads or instabilities.

(5) Solve the Optimization Problem: The optimization problem is solved by utilizing numerical optimization methods such as quadratic programming or linear programming, which take into account the predefined objective function and constraints. This process enables the acquisition of optimal control inputs.

(6) Implement Control Input: The optimized control inputs obtained in the previous step are then implemented on the actual system. As a result, the system's state and output are modified accordingly, marking the transition to the next control cycle.

(7) Loop Control: By continuously repeating the steps above, real-time control and adjustment of the system are achieved, adapting to system changes and meeting control objectives.

The traditional FCS-MPC control algorithm, based on model prediction, iteratively solves the optimization problem to better predict system behavior and dynamically adjust system control inputs. This algorithm offers excellent performance and stability and is widely used in various real-time control systems. The control diagram depicted in Fig. 5 showcases the three-level inverter, which is based on current control FCS-MPC[32-33] .

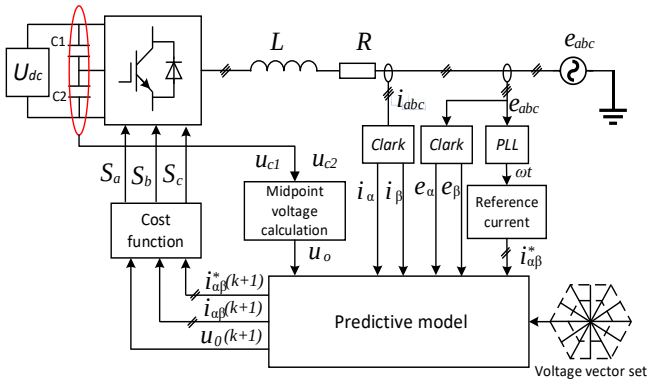

Fig.5. Model Predictive Control Diagram of the Three-Level NPC Inverter

In practice, to compensate for time delays, the predicted current can be further predicted as:

$$\begin{bmatrix} i_\alpha(k+2) \\ i_\beta(k+2) \end{bmatrix} = \frac{Ts}{L}\begin{bmatrix} u_\alpha(k+1)-e_\alpha(k+1) \\ u_\beta(k+1)-e_\beta(k+1) \end{bmatrix} + (1-\frac{RT_s}{L})\begin{bmatrix} i_\alpha(k+1) \\ i_\beta(k+1) \end{bmatrix} \tag{14}$$

The control principle of two-step prediction requires the use of two-step prediction to offset delays, which involves predicting the inverter side current reference value at time k+2. Consequently, it becomes essential to delay compensate the reference value of the inverter side current at time k in order to obtain the inverter side current reference value at time k+2.

The conventional FCS-MPC algorithm, illustrated in Fig. 6, employs an exhaustive enumeration of all possible switch combinations to search for the converter system output switch state combination that minimizes the cost function value. The optimal switch state combination is then utilized in the inverter control algorithm.

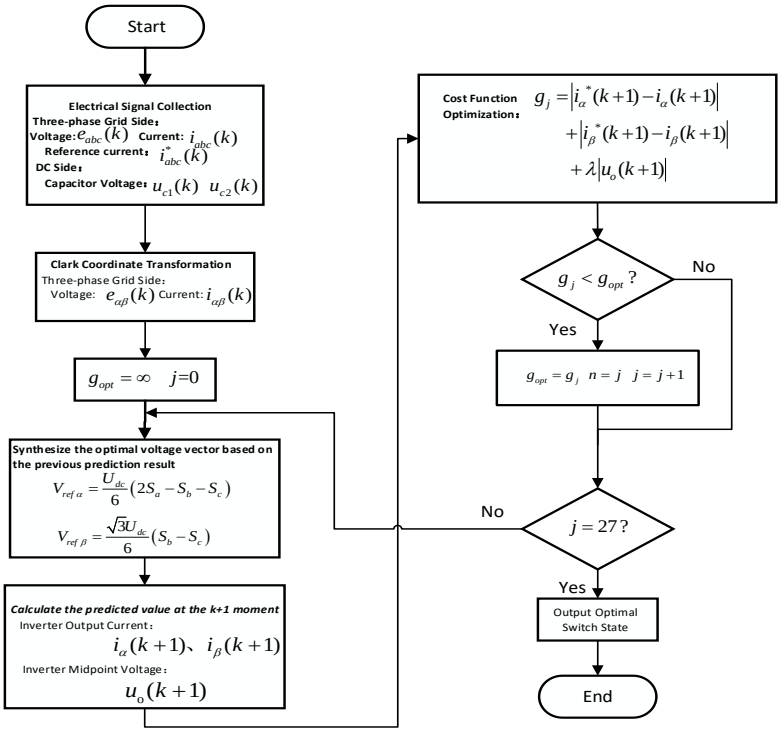

Fig.6. Flowchart of the Traditional FCS-MPC Algorithm for Three-level NPC Inverter

4.2 Sector-based FCS-MPC Control Algorithm

In order to further alleviate the computational burden, particularly for the cost function calculations and prediction model computations related to the upper and lower DC bus voltages, voltage vectors that are significantly different from the inverter output voltage reference vector will be excluded from the optimization calculations.

During a single sampling period, the optimization process comprises 27 cycles. In each cycle, it is necessary to compute the online predicted values for both the inverter-side current and the DC-side midpoint capacitance voltage. These values are then compared by inserting them into the objective function, resulting in a considerable amount of online computations. To lessen the online computational workload, the voltage vectors can be divided into 6 sectors, as depicted in Fig. 7. By determining the sector in which the reference voltage vector falls, only vectors within that sector will be selected for calculation, thus reducing the number of cycles required [34-35].

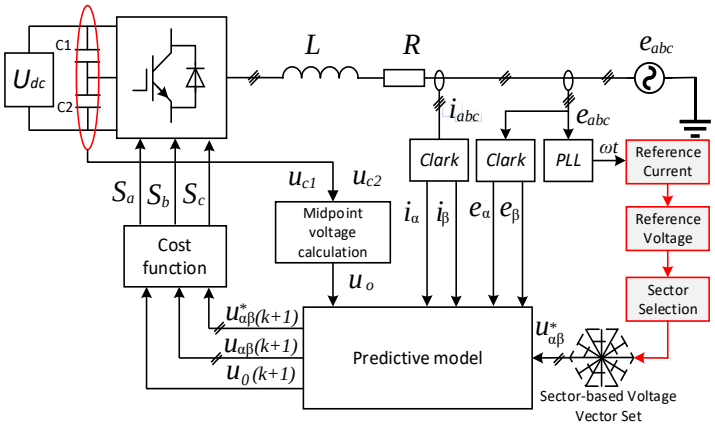

Fig.7. Sector-based Model Predictive Control Diagram for the Three-level NPC Inverter

$$g_j = \left|V_\alpha^*(k+1) - V_\beta(k+1)\right| + \left|V_\beta^*(k+1) - V_\beta(k+1)\right| + \lambda\left|u_o(k+1)\right| \tag{15}$$

From Fig. 3, it is evident that there are redundancies present in the combinations of switch states. The voltage vector corresponding to the zero vector has a magnitude of zero. When any of the 3 sets of zero vectors are output, it does not affect the neutral point voltage. Similarly, the small vectors have the same impact on the midpoint voltage. However, when 6 small vectors are activated, they positively affect the midpoint current, while the remaining 6 small vectors have a negative impact, hence referred to as positive small vectors and negative small vectors. Moreover, the 6 middle vectors also influence the midpoint current, whereas the 6 large vectors do not affect it[36].

The space vector diagram is divided into regions by 60°, divided into six sectors, respectively labeled as I, II, III, IV, V, VI to indicate the sector number, and each sector has an angle of 60°, as shown in Fig. 3.

Upon determining the region of the reference voltage vector, it becomes possible to select a suitable voltage vector that minimizes computational efforts. This approach eliminates the need to calculate cost functions using voltage vectors that are significantly distant from the reference vector, as such vectors are highly unlikely to yield optimal solutions. Consequently, these distant vectors are disregarded and excluded from online evaluations. Table 2 presents the complete set of voltage vectors designated for each sector.

Table 2

Voltage Vector Set by Sector

Sector	Voltage Vector Set by Sector
I	v_1 v_4 v_5 v_{12} v_{13} v_{14} v_{15} v_{16} v_{21} v_{27}
II	v_1 v_{10} v_{11} v_{12} v_{13} v_{14} v_{15} v_{20} v_{21} v_{26}

III	v_1	v_8	v_9	v_{10}	v_{11}	v_{12}	v_{13}	v_{19}	v_{20}	v_{25}
IV	v_1	v_6	v_7	v_8	v_9	v_{10}	v_{11}	v_{18}	v_{19}	v_{24}
V	v_1	v_4	v_5	v_6	v_7	v_8	v_9	v_{17}	v_{18}	v_{23}
VI	v_1	v_4	v_5	v_6	v_7	v_{14}	v_{15}	v_{16}	v_{17}	v_{22}

By rationally selecting sectors, the number of iterations has been simplified. As shown in Fig. 8, it depicts the algorithm flowchart. After determining the sector based on the reference voltage vector, only the 10 voltage space vectors within this sector are used for online calculations. The number of algorithm iterations is reduced from 27 to 10, significantly improving the performance of the control system.

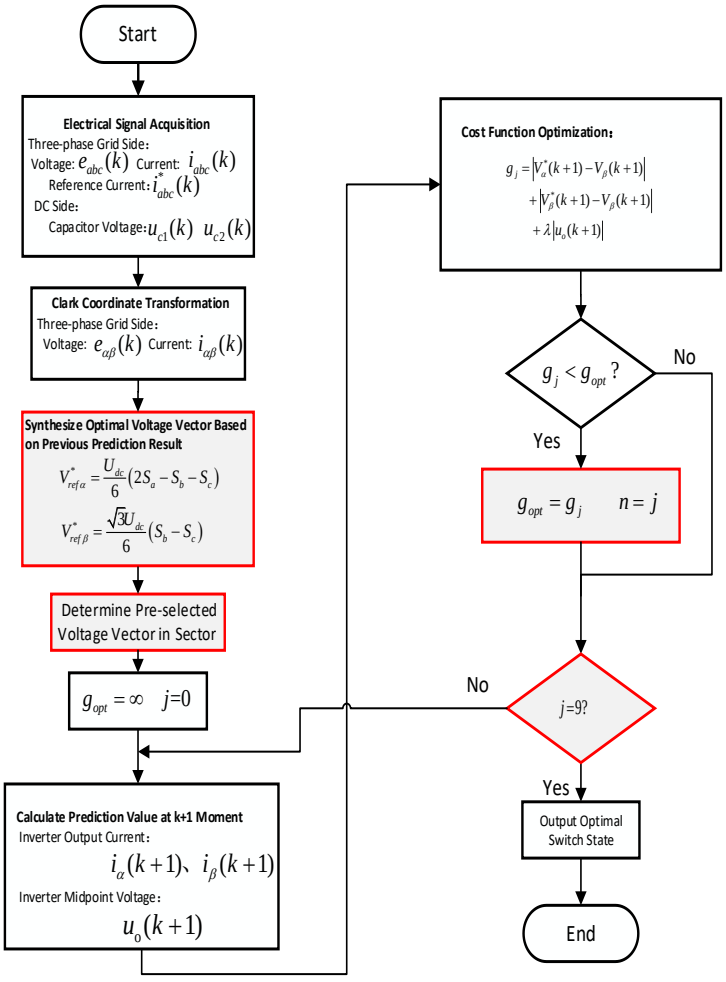

Fig.8. Three-level NPC inverter sector-based model predictive current control flowchart.

5. Simulation Results

To validate the viability of the suggested control strategy, a simulation model for the sector-based FCS-MPC was developed. The simulation was conducted using MATLAB/Simulink, with the simulation parameters detailed in Table 3.

Table 3

Main simulation parameters

Parameters	value
DC bus voltage *udc*	310V
DC side filter capacitors *C1, C2*	1000uF
Grid line voltage peak *e*	150V
Grid frequency *f*	50Hz
Filter inductor *L*	0.02H
Parasitic resistance *R*	0.05Ω
Sampling frequency *fs*	10kHz

5.1 Analysis of Inverter Output Dynamics

In order to investigate the dynamic response performance of the enhanced FCS-MPC, the reference current amplitude was deliberately varied between 10A and 15A. The time-domain simulation in Fig. 8 demonstrates that at 0.05 seconds, the inverter output current swiftly rises from a peak value of 10A to 15A. Similarly, at 0.1 seconds, the current promptly drops back to 10A. Notably, in both scenarios, the inverter effectively tracks the desired three-phase current, thereby ensuring system stability. The simulation unequivocally attests to the rapid dynamic response exhibited by the improved FCS-MPC methodology.

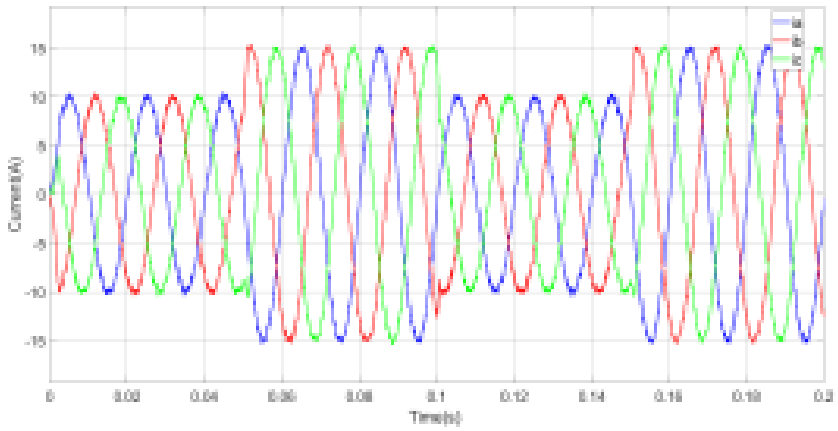

Fig.9. Inverter Grid Waveform

5.2 Analysis of Inverter Neutral Point Voltage Balancing Capability

To highlight the midpoint voltage suppression capability of the proposed method, simulations were conducted for cost function voltage balance part weight coefficients λ=10, λ=0.6, and λ=0.

As shown in Fig. 9, when λ=10, the simulation results indicate that the voltages across capacitors C1 and C2 alternate over time, fluctuating within a controllable range. The composite midpoint voltage is relatively small, as shown in Fig. 10, minimally impacting the grid system. Hence, it can be inferred that at λ=10, this weight coefficient reflects the influence of midpoint voltage magnitude on the overall control system.

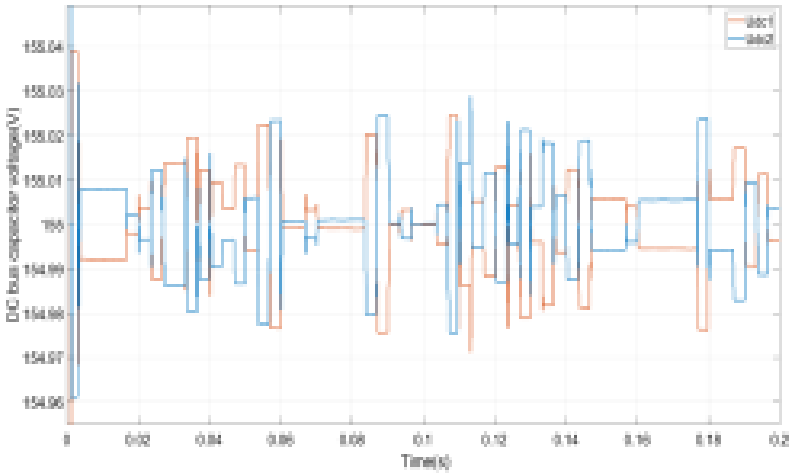

Fig.10. Voltage waveform of Udc1 and Udc2 at λ=10

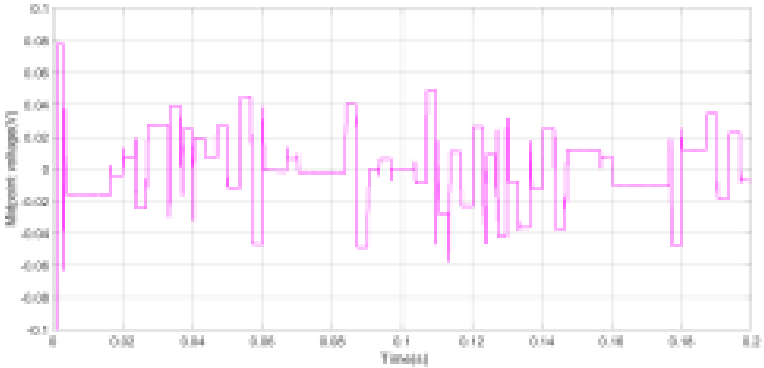

Fig.11. Midpoint voltage waveform at λ=10

As depicted in Fig. 11, when λ=0.6, simulation results demonstrate that the voltages across capacitors C1 and C2 alternate with time, with an increased amplitude. The resulting midpoint voltage noticeably rises, and as Fig. 12 illustrates, the midpoint voltage fluctuates considerably, amplifying its impact on the grid system. Therefore, it can be inferred that at λ=0.6, under this weight coefficient, the control system's capability to optimally regulate the midpoint voltage weakens. In order to achieve optimal system control performance and effectively suppress midpoint voltage, it is necessary to select appropriate weight coefficients.

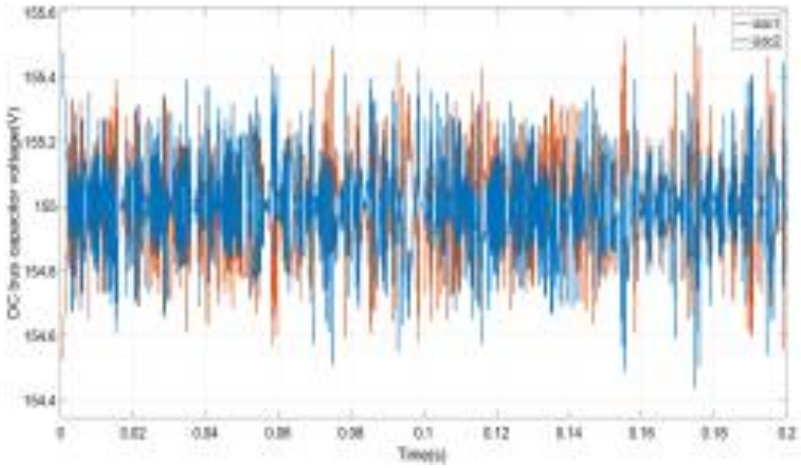

Fig.12. Voltage waveform of Udc1 and Udc2 at λ=0.6

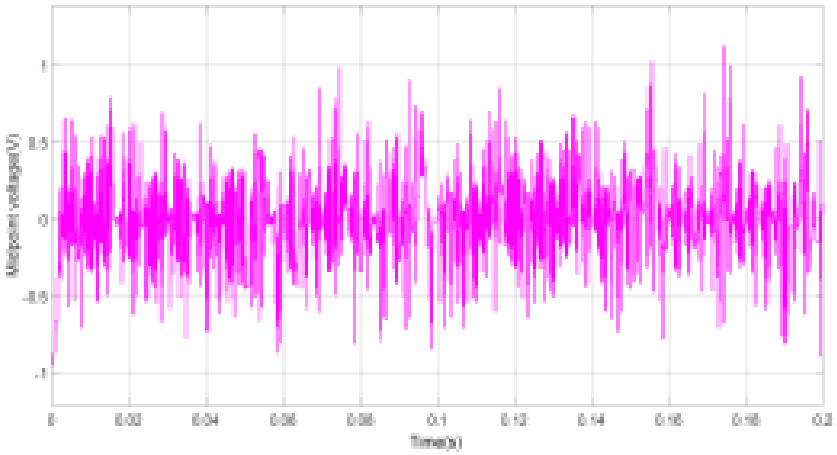

Fig.13. Midpoint voltage waveform at λ=0.6

As seen in Fig. 13, when λ=0, the simulation results suggest that the voltages across capacitors C1 and C2 begin to increase, reaching a peak at 0.2 seconds. The resulting midpoint voltage is high, considerably affecting the grid system. Thus, it underscores the significance of integrating a midpoint voltage suppression algorithm.

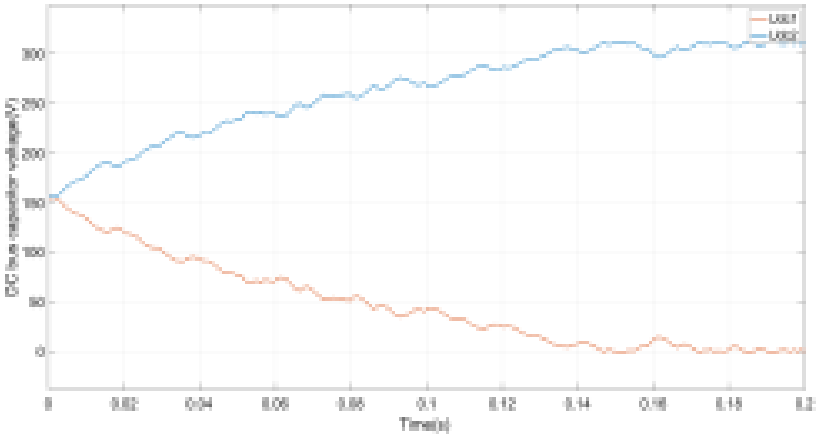

Fig.14. Voltage waveform of Udc1 and Udc2 at λ=0

Simulations of the midpoint voltage waveform were conducted under various weight coefficients, yielding diverse results, suggesting the algorithm's midpoint voltage balancing ability depends on the weight coefficient of the midpoint voltage function.

5.3 Inverter Grid Current Harmonic Analysis

For the simulation system, when the grid current was 10A, a Fast Fourier Transform (FFT) analysis was performed, yielding a Total Harmonic Distortion (THD) of 2.59%. As displayed in Fig. 14, it meets the requirements for grid connection. A FFT analysis was also executed when the grid current was 15A, resulting in a THD of 1.98%. This too satisfies grid connection criteria. The simulation waveforms and FFT analysis results of the midpoint voltage-weighted optimized FCS-MPC method demonstrate that the control strategy effectively enhances grid current quality.

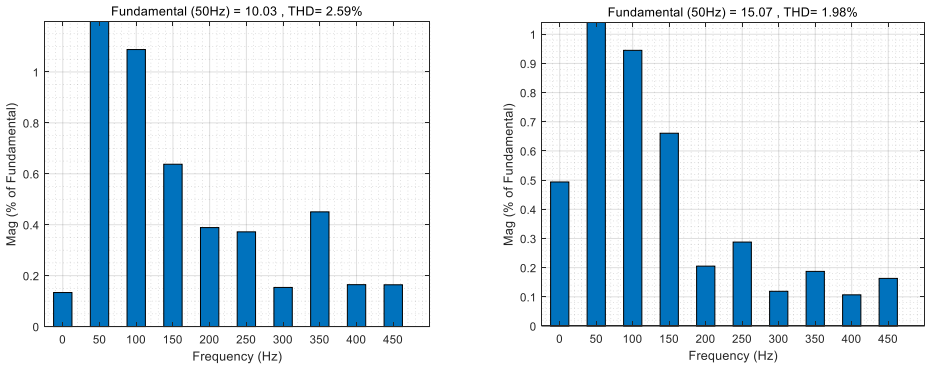

Fig.15. Fundamental current amplitude 10A THD | Fundamental current amplitude 15A THD

6. Conclusion

This work proposes a finite-set model predictive control strategy for a three-level grid-connected converter under midpoint voltage balance. By integrating the finite-set switch state model with predictive control, precise control and balancing of the grid-side midpoint voltage have been realized. Key achievements of this study include establishing a mathematical model for the three-level grid-connected converter, introducing a finite-set switch state model to describe system behavior, and designing a sector-based simplified model predictive control algorithm to achieve closed-loop control of the output current. The effectiveness and feasibility of the proposed method were validated through simulation experiments, accurately controlling voltage and current while suppressing midpoint voltage imbalance. This research holds significant importance for enhancing the control performance and output quality of three-level grid-connected converters. Future research directions could involve optimizing the predictive control algorithm, considering real-time grid environments and load changes to further enhance control precision and response speed. Additionally, integrating this strategy with other advanced control techniques could bolster system robustness and stability. Implementing and verifying the proposed control strategy on actual hardware could further affirm its feasibility and practicality. Limitations of this study lie in further refining and optimizing the control strategy to meet varying operational conditions and application requirements.

Acknowledgements

This work is supported by Special projects in key fields for higher education of Guangdong province [grant number 2021ZDZX3008].

REFERENCES

[1] Guo Leilei, Jin Nan, Xu Lie. Inverter common mode voltage spike elimination method using hybrid voltage vector pre-selection and reference voltage prediction. Chinese Journal of Electrical Engineering, 2018, 38(17): 5167-5176, 5314.

[2] Energy; University of sevilla researchers provide new study findings on energy (efficient fpsoc prototyping of fcs-mpc for three-phase voltage source inverters). Energy weekly news, 2020.

[3] Electronics; new findings from Jiangsu university in the area of electronics described (fcs-mpc-based fault-tolerant control of five-phase ipmsm for mtpa operation). Electronics newsweekly, 2020.

[4] Electronics; new findings from jiangsu university in the area of electronics described (fcs-mpc-based fault-tolerant control of five-phase ipmsm for mtpa operation). Electronics newsweekly, 2020.

[5] Aguirre Matias, Kouro Samir, Rojas Christian Alexis, et al. Enhanced switching frequency control in fcs-mpc for power converters. IEEE Transactions on Industrial electronics, 2020.

[6] Zhu Chenghao, Wang Han, Sun Guoqi, et al. A DC Capacitance identification Method for Grid-connected inverters. Journal of Shanghai Jiao Tong University, 2022, 56(06): 693-700.

[7] Mohammed Alhasheem, Paolo Mattavelli, Pooya Davari. Harmonics mitigation and non-ideal voltage compensation utilizing active power filter based on predictive current control. IET Power Electronics, 2020, 13(13).

[8] Zhang Yongchang, Yang Haitao. Asynchronous motor model predictive control without speed sensor. Chinese Journal of Electrical Engineering, 2014, 34(15): 2422-2429.

[9] Bi Enzi, Yang Jianfeng, Liu Yang, et al. Multistep finite-control-set model predictive control of active power filter. IOP Conference Series: Earth and Environmental Science, 2020, 617(1).

[10] Liu Guohai, Song Chengyan, Chen Qian. FCS-MPC-based fault-tolerant control of five-phase ipmsm for mtpa operation. IEEE Transactions on Power Electronics, 2020, 35(3).

[11] Yanhong Luo, Songsheng Wang, Dongsheng Yang, et al. Direct prediction compensation strategy of unified power quality conditioner based on fcs-mpc. IET Generation Transmission & Distribution, 2020, 14(22).

[12] Yifeng Zhu, Hao Yue, Hailong Zhao, et al. Improved model predictive current control of single-phase five-level pwm rectifier. Energies, 2020, 13(9).

[13] Eduardo Zafra, Sergio Vazquez, Hipolito Guzman Miranda, et al. Efficient fpsoc prototyping of FCS-MPC for three-phase voltage source inverters. Energies, 2020, 13(5).

[14] Meng Hui, Guo Qiufen, Ren Shenhe. TPESFTI drive DFIG system FCS-MPC based on sliding mode control. Micro Motor, 2020, 48(05): 56-61.

[15] He Ting, Qiao Junqiang, Bao Jianqin, et al. Comparative study of FCS-MPC and CCS-MPC for permanent magnet synchronous motors. Micro Motor, 2020, 53(10): 52-57, 93.

[16] Liu Yun, Xiao Huafeng, Shi Mingming, et al. Proceedings of the CSEE, 2023, 43(17): 6796-6807. Three-five-level Dual-mode Soft-Switch Common Ground Non-isolated Grid-connected Inverter.

[17] Mohamed Azab. A finite control set model predictive control scheme for single-phase grid-connected inverters. Renewable and sustainable energy reviews, 2021, 135.

[18] Gao Chong, Huang Yuansheng, Wang Hongwei. Research on the flexible multi-state power source switch high ratio power distribution model based on FCS-MPC. Journal of Power Supply, 2022, 20(04): 131-137.

[19] Xiao Zhang, Li Tan, Jiaheng Xian, Hui Zhang, Zhixun Ma, Jinsong Kang. Direct grid-side current model predictive control for grid-connected inverter with LCL filter. IET power electronics, 2018

[20] Babqi Abdulrahman J., Alamri Basem. A comprehensive comparison between finite control set model predictive control and classical proportional-integral control for grid-tied power electronics devices. Acta Polytechnica Hungarica, 2021, 18(7).

[21] Li Fei, Liu Zhan, Zhao Qiang, et al. Simplified fixed-frequency PWM three-level rectifier control strategy based on model prediction. Journal of Electric Power Science and Technology, 2021, 36(02): 116-123.

[22] Zhou Xuesong, Liu Qian, Ma Youjie, et al. Dc bus Voltage control of grid-connected photovoltaic inverters based on improved active disturbance rejection. Acta Solar Energy Sinica, 2022, 43(10): 65-72.

[23] Liu Qiyu, LI Yonggang, WANG Yue, et al. Grey box impedance identification and impedance polymerization Analysis method for multi-grid-connected Inverter System. Electric Power Automation Equipment, 2022, 42(11): 92-98, 105.

[24] Zhang Shulin, Kang Jinsong, Sheng YeZhe. A three-level NPC inverter low common-mode voltage FCS-MPC algorithm without weight coefficients. Chinese Journal of Electrical Engineering: 1-13.

[25] Wang Xiawa, Wang Yan, Yan Qi. NPC type three-level photovoltaic grid-connected inverter model predictive control. Electrical Drive Automation, 2019, 41(04): 26-31, 17

[26] Teng Li, Xiaodong Sun, Gang Lei, et al. finite-control-set model predictive control of permanent magnet synchronous motor drive systems—an overview. OEEE/CAA journal of automatica sinica, 2022, 9(12): 2087-2105.

[27] Wang Jinlong, ZHAO Haoran, Wang Peng, et al. Analysis and Improvement of Small Signal Stable Power Limit of grid-connected Inverters Based on Impedance Method. Power System Protection and Control, 2022, 50(18): 18-28.

[28] Cai Yuhan, Yan Shaomin, Cui Yue, et al. Single-loop control method FCS-MPC for pmsg. ieice electronics express, 2023, 20(1).

[29] Xu Wei. Research on FCS-MPC for lc filter inverter. Academic journal of engineering and technology science, 2023, 6(6).

[30] Wang Yufeng, Zhang Hongmei, Yin Yuwei. Study on suppressing resonance in HAPF reactive power compensation control by FCS-MPC. Measurement and Control Technology, 2021, 40(06): 100-106, 113.

[31] Tao Hongwei, Peng Tao, Yang Chao, et al. An FCS-MPC-based open-circuit and current sensor fault diagnosis method for traction inverters with two current sensors. International journal of electrical power and energy systems, 2023, 144.

[32] Saberi Sajad, Rezaie Behrooz. Direct speed control of pmsg-based airborne wind energy system using FCS-MPC method. ISA transactions, 2022, 131.

[33] Wang Wei, Chen Hongmin, Jin Yuhang, et al. Multi-objective coordinated control method of grid-connected Inverter based on sliding window DFT algorithm. Power System Protection and Control, 2022, 50(09): 145-151.

[34] Yu Yanxue, Hu Pengfei, Chen Yushu, et al. Analysis and improvement method of Power Transmission capability of grid-connected inverters in Extremely Weak Current Network. Automation of Electric Power Systems, 2022, 46(14): 101-108.

[35] Stoji Djordje, Rivera Marco. New hysteresis fcs-mpc ac current controller with disturbance estimator. Electrical engineering, 2023, 105(4).

[36] Liu Xing, Qiu Lin, Wu Wenjie, et al. finite-time eso-based cascade-free fcs-mpc for nnpc converter. International journal of electrical power and energy systems, 2023, 148.